

Electron and Nucleon Localization Functions in Superheavy Elements

Paul Jerabek,¹ Bastian Schuetrumpf,² Peter Schwerdtfeger,¹ and Witold Nazarewicz³

¹*Centre for Theoretical Chemistry and Physics, The New Zealand Institute for Advanced Study, Massey University Auckland, 0632 Auckland, New Zealand*

²*NSCL/FRIB Laboratory, Michigan State University, East Lansing, Michigan 48824, USA*

³*Department of Physics and Astronomy and FRIB Laboratory, Michigan State University, East Lansing, Michigan 48824, USA*

Fermion localization functions are used to discuss electronic and nucleonic shell structure effects in superheavy elements, including the element Oganesson, the heaviest element discovered to date. Spin-orbit splitting in the $7p$ electronic shell becomes so large (~ 10 eV) that Og shows Fermi-gas-like behavior with a rather large dipole polarizability compared to the lighter rare gas elements. The nucleon localization in superheavy nuclei is predicted to undergo a transition to the Fermi-gas-like behavior as well. This effect, particularly strong for neutrons, is due to the high density of nucleonic orbitals and strong polarization effects.

Introduction – Oganesson ($Z = 118$) is the recent addition to the Periodic Table of the Elements and the Chart of Nuclides [1]. The isotope $^{294}_{118}\text{Og}$ was produced in a heavy ion fusion reaction with a $^{48}_{20}\text{Ca}$ beam and a $^{249}_{98}\text{Cf}$ target [2, 3]. The heaviest element studied chemically to date is Fl ($Z = 114$). Its relatively long half-life, 1-2 s, enables chemical studies with ~ 5 atoms/day, which marks the limit of chemistry today [4, 5]. The estimated α -decay half-life of $^{294}_{118}\text{Og}$, $0.89^{+1.07}_{-0.31}$ ms, is too short for chemical “one-atom-at-a-time” studies; hence, its chemical properties must be inferred from advanced atomic calculations based on relativistic quantum theory [6–19]. According to these, Og has a closed-shell $[\text{Rn}]5f^{14}6d^{10}7s^27p^6$ configuration [13, 20, 21], with a very large spin-orbit splitting of the $7p$ shell (9.920 eV at the Dirac-Breit-Hartree-Fock and 10.125 eV at the Fock-Space Coupled-Cluster level, see below). While – according to its electronic configuration – Og completes the 7th row of the Periodic Table, it does not behave like a typical rare gas element. For example, the relativistic $7p_{3/2}$ expansion and the relativistic $8s$ contraction make Og the first rare gas element with a positive electron affinity of 0.064 eV [10, 16, 22]. This result includes a substantial quantum electrodynamic correction of 0.006 eV [16].

Nuclear structure calculations predict ^{294}Og to be a deformed nucleus [23–26], eight neutrons away from the next neutron shell closure at ^{302}Og ($N = 184$) [27–32]. A new factor impacting properties of superheavy nuclei is the strong electrostatic repulsion: the Coulomb force in superheavy nuclei cannot be treated as a small perturbation atop the dominating nuclear interaction; the resulting polarization effects due to Coulomb frustration are expected to influence significantly proton and neutron distributions and shell structure [26, 28, 31, 33–37]. In particular, the isotope $^{294}_{118}\text{Og}$ is believed to be a semi-bubble system with a sizable central depression of the proton density [26].

The objective of this paper is to study the electronic and nucleonic shell structure of superheavy elements. To this end, we utilize the fermion localization measure [38],

which is an excellent indicator of shell structure. In particular, we investigate the transition from the regime of strong localization, governed by shell effects, to a delocalized regime typical of the homogenous Fermi gas. As we shall demonstrate below, superheavy atoms and nuclei constitute an excellent territory where to look for such a transition.

Fermion localization function – The spatial localization measure was originally proposed in atomic and molecular physics to characterize chemical bonding in electronic systems [38–43]. It has been subsequently introduced to nuclear physics to visualize cluster structures in light nuclei [44] and has also been applied to nuclear fission [45] and to nucleonic matter in the inner crust of neutron stars [46]. In electronic systems, it is referred to as the electron localization function (ELF), in nuclear systems as the nucleon localization function (NLF). It is based on the inverse of the conditional probability of finding a fermion of type q ($= e, n, \text{ or } p$) in the vicinity of another fermion of the same type and same spin/signature quantum number σ ($= \uparrow$ or \downarrow), knowing that the latter particle is located at position \mathbf{r} . In the non-relativistic case, the localization measure is

$$\mathcal{C}_{q\sigma}(\mathbf{r}) = \left[1 + \left(\frac{\tau_{q\sigma}\rho_{q\sigma} - \frac{1}{4}|\nabla\rho_{q\sigma}|^2 - \mathbf{j}_{q\sigma}^2}{\rho_{q\sigma}\tau_{q\sigma}^{\text{TF}}} \right)^2 \right]^{-1}, \quad (1)$$

where $\rho_{q\sigma}$, $\tau_{q\sigma}$, $\mathbf{j}_{q\sigma}$, and $\nabla\rho_{q\sigma}$ are the particle density, kinetic energy density, current density, and density gradient, respectively. $\tau_{q\sigma}^{\text{TF}}$ denotes the Thomas-Fermi kinetic energy. In this work, time reversal symmetry is conserved; hence, $\mathbf{j}_{q\sigma}$ vanishes.

The localization function takes generally values between 0 and 1. A value close to 1 indicates that the probability of finding two particles (of the same type) close to each other is very low. Thus a high value of \mathcal{C} marks the spatial regions corresponding to shell separations. Since the localization function (1) is normalized to the Thomas-Fermi kinetic energy, $\mathcal{C} = 1/2$ corresponds to a limit of the homogeneous Fermi gas, in which the

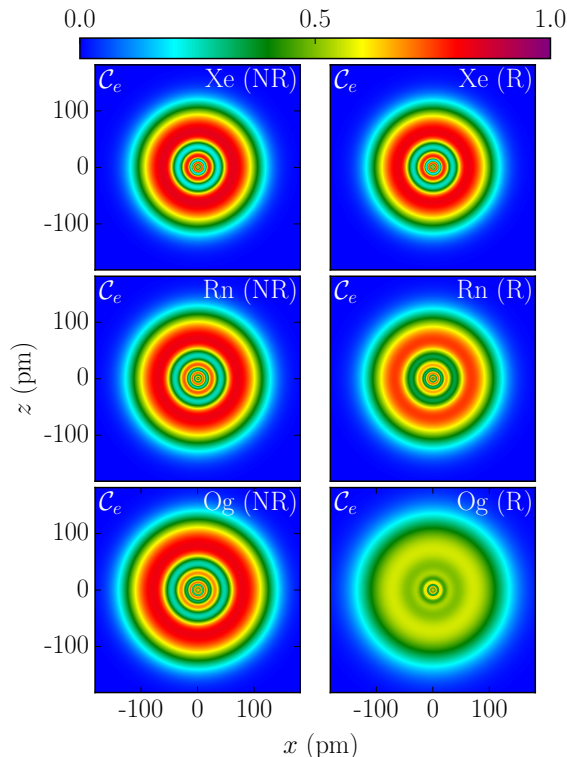


FIG. 1. ELFs from nonrelativistic (NR, left) and Dirac-Hartree-Fock calculations (R, right) for the heavy rare gas atoms Xe (top), Rn (middle), and Og (bottom).

individual orbits are spatially delocalized.

Electron localization – For the electronic structure calculations we used the ELF module as implemented in the relativistic ab-initio quantum chemistry program DIRAC15 [47]. Hartree-Fock one-particle densities were generated in non-relativistic, scalar-relativistic (module x2C-spinfree) [48, 49], and (4-component) Dirac-Coulomb calculations in conjunction with an uncontracted relativistic quadruple-zeta basis set DYALL.ACIV4Z [50]. The Dirac-Fock computations include the small-component integrals as well as the two-electron Gaunt term. We utilized the finite-field method to compute the static electric dipole polarizability of Og (with external electric field strengths of 0.0, 0.0005 and 0.001 a.u.) at CCSD(T) Coupled-Cluster level,[12] which included excitations from singles, doubles, and perturbative triples. In the correlation treatment, we included 50 electrons and virtual orbitals up to 25 a.u. Here we used the molecular mean-field x2C Hamiltonian [51] with the Gaunt term included. Fock-Space Coupled-Cluster calculations [16] were carried out to obtain the ionization potentials from the filled $7p_{3/2}$ and $7p_{1/2}$ shells of Og. Note, that only large-component densities are considered for the non-relativistic and scalar-relativistic ELF, whereas in the 4-component case the small-component densities are added to the large-components to yield the

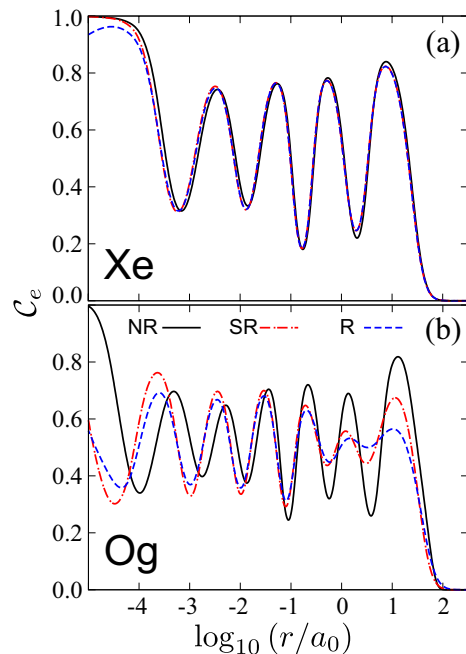


FIG. 2. ELFs for Xe (a) and Og (b) from non-relativistic (NR), scalar-relativistic (SR), and Dirac-Hartree-Fock (R) calculations as a function of the distance from the nucleus. The relativistic contraction of inner shells and smearing out of the shell structure in the valence and sub-valence shells of Og are clearly seen.

total one-particle density.

Figures 1 and 2 show the ELFs predicted in our calculations. As seen in Fig. 1, electron localizations for Xe or Rn hardly change from the nonrelativistic to the 4-component relativistic framework. However, for Og we see significant electron delocalization with ELF values that are much smaller compared to the non-relativistic case, making the atomic shell structure barely recognizable. The pattern of concentric rings is a fingerprint of the underlying shell structure. The sizes of rings in ELF reflect the radii of electron orbits in different shells; hence, they roughly scale as $\sim n^2$, where n is the principal quantum number. Figure 2(b) clearly shows that the delocalization is due to spin-orbit coupling and not due to scalar relativistic effects. This results in an evenly distributed ELF with values around 0.5 in the outer shells. The valence and sub-valence shells of Og are, therefore, smeared out like in a homogenous electron gas. Rn behaves similarly to Xe, although some delocalization through relativistic effects is already apparent.

A more detailed analysis shows that smearing out of the electron density in the valence region originates from the strong spin-orbit splitting of the $7p$ shells; while the radii for the valence $5p$ orbitals in Xe are very similar (2.239 and 2.141 a.u. for $5p_{3/2}$ and $5p_{1/2}$, respectively, as obtained with the numerical program GRASP92 [52]) the $7p_{3/2}$ shell in Og is 0.75 a.u. further out compared to

the $7p_{1/2}$ shell (2.796 and 2.039 a.u., respectively). Large spin-orbit splittings are also calculated for the lower lying $\ell > 0$ (core) shells. Further, the density of the single-particle (s.p.) states increases from Xe to Og as expected for higher principal quantum numbers, see Figure 3. As a result of these effects, the electron density is more homogeneously distributed over the entire atomic range, i.e., less localized, resulting in ELF values oscillating around the Fermi-gas limit. The Fock-Space Coupled-Cluster calculation gave ionization potentials of $7p_{3/2}$ and $7p_{1/2}$ of 8.842 and 18.967 eV, respectively, thus spin-orbit splitting for the valence $7p$ orbital of Og is extremely large (10.125 eV). Figure 3 illustrates this in relation to the orbital energy levels of the lighter homologues.

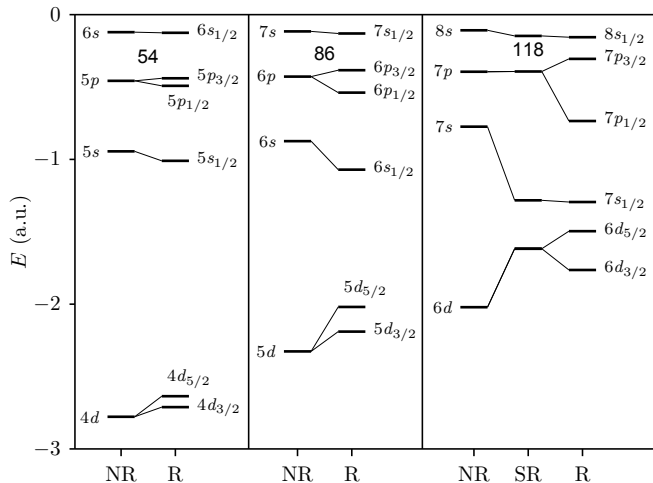


FIG. 3. Orbital energy levels of Xe (left), Rn (middle), and Og (right) for the 1S_0 ground state as obtained from non-relativistic (NR) and scalar-relativistic (SR) Hartree-Fock and Dirac-Hartree-Fock (R) calculations. $6s$ (Xe), $7s$ (Rn), and $8s$ (Og) orbital energies taken from the first excited 3P_2 state.

According to the Thomas-Fermi model, the static dipole polarizability $\alpha \sim r_a^3$, with r_a^3 being the atomic radius [53]. The electron-gas-like outer shell of Og is thus much easier to polarize ($\alpha = 57.98$ a.u.) as compared to xenon ($\alpha = 27.815$ a.u. [54]) or radon ($\alpha = 33.18$ a.u. [55]). For comparison, the nonrelativistic and scalar relativistic values for Og are $\alpha = 45.30$ a.u. and $\alpha = 43.78$ a.u., respectively. Thus, for Og one expects an increase in van-der-Waals interactions compared to the lighter rare gases, and subsequently a significant change in chemical and physical properties of this element, which has already been pointed out in Refs. [10–12, 15, 19, 56].

Nucleon localization – For the nuclear calculations, we employ nuclear density functional theory [57] with carefully optimized global Skyrme energy density functionals UNEDF1 [58] and SV-min [59]. Pairing is treated at the BCS level. We use the DFT solver of Ref. [60] constrained to spherical geometry.

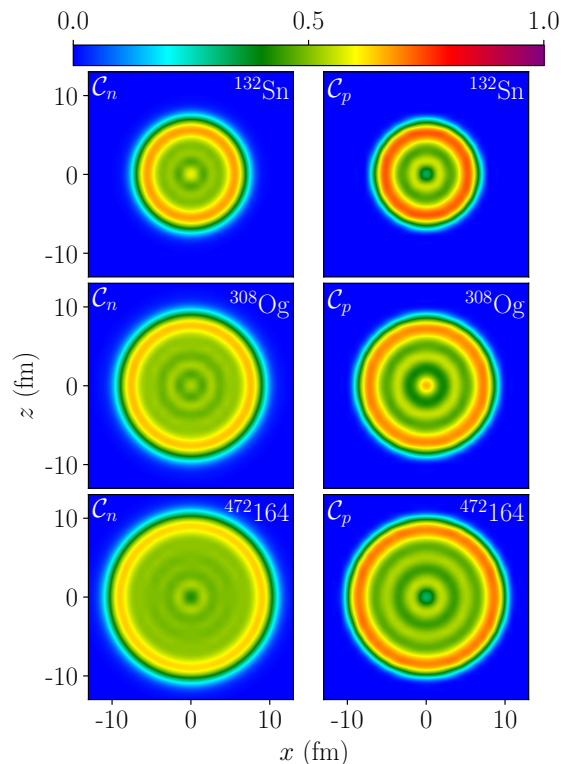


FIG. 4. NLFs of ^{132}Sn , ^{302}Og , and $^{472}164$ calculated with the energy density functional UNEDF1.

Figure 4 shows the NLFs for the doubly magic medium-mass nucleus ^{132}Sn and spherical superheavy systems ^{302}Og and $^{472}164$. In contrast to the ELFs, the number of closed shells cannot be determined from the number of radial maxima. This is due to the different radial behavior of single-nucleon orbits. While the radii of electron orbits in atoms belonging to different shells are spatially well separated, radii of nucleonic orbits scale as $\sim \sqrt{2n + \ell}$, i.e., they very gradually increase with the shell number. This results in a large spatial overlap between single-nucleon wave functions and reduced localizations as compared to the electronic case.

Inspecting the NLFs of protons to neutrons, one notes that the patterns of concentric rings is more distinct in the proton system, as the number of occupied proton shells is less than that for the neutrons, within the same volume (as the rms proton and neutron radii are very similar [24]). This effect becomes fairly pronounced for superheavy nuclei where the neutron excess is large. While the NLF for the medium-mass nucleus ^{132}Sn exhibits a clear shell structure with distinct oscillations around $C = 0.5$ [45], the maxima and minima become fainter for heavier systems. This is particularly striking for the neutrons. While the neutron NLF for ^{302}Og still exhibits a faint structure in the interior, the ring pattern almost vanishes for $^{472}164$. Furthermore, the maximum in the surface area becomes fainter for the heavy systems.

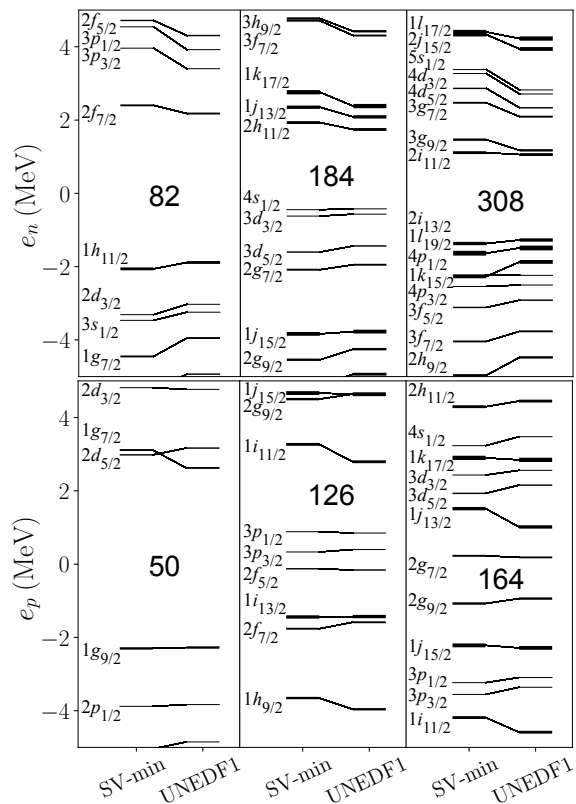


FIG. 5. Neutron (top) and proton (bottom) Hartree-Fock energies relative to the Fermi energy predicted with SV-min and UNEDF1 for ^{132}Sn (left), ^{302}Og (middle), and $^{472}164$ (right). The line thickness is proportional to the orbital's degeneracy $2j + 1$.

Overall, as mass increases, the neutron localization approaches the Fermi gas limit $\mathcal{C} = 0.5$. The NLF pattern seen in Fig. 4 reflects the underlying nucleonic shell structure. As discussed in, e.g., Refs. [27–32] the general pattern of s.p. energies undergoes significant changes in superheavy nuclei. First, the s.p. level density is large; in fact it grows faster than $A^{1/3}$ [32]. Consequently – similar to what has been discussed earlier in the context of atomic calculations of the electron shell structure of superheavy elements – small changes in the theoretical description can impact shell structure substantially. Second, the shell structure of superheavy nuclei is influenced by the self-consistent interplay between the short-range attractive nuclear force and the long-range electrostatic repulsion. Thanks to this highly non-perturbative Coulomb rearrangement (or frustration), significant rearrangements of nucleonic densities, such as the appearance of central depression, are predicted [26, 28, 31, 33–37]. The presence of central depression strongly affects high- j orbits due to their large s.p. radii [27, 31, 34, 36].

Figure 5 shows single-nucleon energy levels for ^{132}Sn , ^{302}Og , and $^{472}164$ obtained with SV-min and UNEDF1 (see also Refs. [29, 30, 32] for predictions of other mod-

els). Both functionals yield fairly similar results for superheavy systems, in spite of huge extrapolations in mass and charge involved. The diagrams for ^{132}Sn illustrate the s.p. level pattern characteristic of nuclei up to ^{208}Pb : large magic gaps (here $Z = 50$ and $N = 82$) that separate nuclear shells consisting of several normal-parity orbits and one unusual-parity high- j intruder state. This familiar pattern becomes modified in superheavy nuclei resulting in the regions of shell-stabilized nuclei that are poorly localized in particle number [29]. For $^{472}164$, several high- j shells cluster below, and directly above, the $N = 308$ and $Z = 164$ gaps; this is consistent with a semi-bubble structure of this system. In the case of ^{302}Og , several low- j shells appear around the Fermi level, which results in a quantum stabilization of this system.

Conclusions – To study electronic and nucleonic shell structure in superheavy elements, we employed the spatial localization measure. The atomic calculations were carried out for heavy rare gas atoms Xe, Rn, and the superheavy element Og recently added to the Periodic Table. The nuclear calculations were performed for the known doubly-magic system ^{132}Sn and for superheavy nuclei ^{302}Og , and $^{472}164$.

Relativistic effects significantly impact the electronic structure of superheavy atoms. For the element Og, the electron shells with $\ell > 0$ show very large spin-orbit splittings smearing out of the one-particle density, thus becoming more homogeneously distributed over the entire atom approaching the electron-gas regime. A direct consequence of this transition is its predicted large static dipole polarizability resulting in an increase in van-der-Waals interactions compared to the lighter rare gases and a significant change in its chemical and physical properties.

A similar transition towards the Fermi-gas regime is predicted for neutron localizations in superheavy nuclei. Proton localizations exhibit shell-structure imprints, even for $Z = 164$, due to the Coulomb rearrangement effects resulting in the central depression of particle densities favouring occupation of higher angular momentum states. In general, neutrons are more delocalized than protons as for the superheavy nuclei N is much greater than Z , i.e., more neutrons are confined to the same volume than protons.

In summary, we predict that Og with $Z = 118$ is a rather unusual addition to the Periodic Table and to the Chart of Nuclides. High density of electronic and nucleonic s.p. states, relativistic effects resulting in the strong spin-orbit splitting of electronic levels, and polarization effects due to strong electrostatic repulsion, make the superheavy atoms, such as Og, quantitatively different from the lighter species.

We acknowledge financial support by the Alexander-von-Humboldt Foundation (Bonn, Germany) and the Marsden Fund of the Royal Society of New Zealand. This work was also supported by the U.S. Department

of Energy, under Award Numbers DOE-DE-NA0002847 (NNSA, the Stewardship Science Academic Alliances program) and DE-SC0013365 (Office of Science).

-
- [1] P. Karol, R. Barber, B. Sherrill, E. Vardaci, and T. Yamazaki, *Pure Appl. Chem.* **88**, 155 (2016).
- [2] Y. T. Oganessian *et al.*, *Phys. Rev. C* **74**, 044602 (2006).
- [3] Y. Oganessian, *Pure Appl. Chem.* **78**, 889 (2006).
- [4] C. E. Düllmann, *Nucl. Phys. News* **27**, 14 (2017).
- [5] A. Türler, R. Eichler, and A. Yakushev, *Nucl. Phys. A* **944**, 640 (2015).
- [6] K. S. Pitzer, *J. Chem. Soc., Chem. Commun.*, 760b (1975).
- [7] K. S. Pitzer, *J. Chem. Phys.* **63**, 1032 (1975).
- [8] P. Pyykkö, *Chem. Rev.* **88**, 563 (1988).
- [9] C. S. Nash and B. E. Bursten, *Angew. Chem. Int. Ed.* **38**, 151 (1999).
- [10] I. Goidenko, L. Labzowsky, E. Eliav, U. Kaldor, and P. Pyykkö, *Phys. Rev. A* **67**, 020102 (2003).
- [11] C. S. Nash, *J. Phys. Chem. A* **109**, 3493 (2005).
- [12] V. Pershina, A. Borschevsky, E. Eliav, and U. Kaldor, *J. Chem. Phys.* **129**, 144106 (2008).
- [13] P. Pyykkö, *Phys. Chem. Chem. Phys.* **13**, 161 (2011).
- [14] O. Kullie and T. Saue, *Chem. Phys.* **395**, 54 (2012).
- [15] A. Türler and V. Pershina, *Chem. Rev.* **113**, 1237 (2013).
- [16] E. Eliav, S. Fritzsche, and U. Kaldor, *Nucl. Phys. A* **944**, 518 (2015).
- [17] P. Schwerdtfeger, L. F. Pašteka, A. Punnett, and P. O. Bowman, *Nucl. Phys. A* **944**, 551 (2015).
- [18] V. Pershina, *Nucl. Phys. A* **944**, 578 (2015).
- [19] A. Shee, S. Knecht, and T. Saue, *Phys. Chem. Chem. Phys.* **17**, 10978 (2015).
- [20] J. P. Desclaux, *At. Data Nucl. Data Tables* **12**, 311 (1973).
- [21] P. Indelicato, J. P. Santos, S. Boucard, and J.-P. Desclaux, *Eur. Phys. J. D* **45**, 155 (2007).
- [22] E. Eliav and U. Kaldor, *Phys. Rev. Lett.* **77**, 5350 (1996).
- [23] S. Ćwiok, P.-H. Heenen, and W. Nazarewicz, *Nature* **433**, 705 (2005).
- [24] J. Erler, N. Birge, M. Kortelainen, W. Nazarewicz, E. Olsen, A. M. Perhac, and M. Stoitsov, *Nature* **486**, 509 (2012).
- [25] P.-H. Heenen, J. Skalski, A. Staszczak, and D. Vretenar, *Nucl. Phys. A* **944**, 415 (2015).
- [26] B. Schuetrumpf, W. Nazarewicz, and P.-G. Reinhard, *arXiv:1706.05759* (2017).
- [27] S. Ćwiok, J. Dobaczewski, P.-H. Heenen, P. Magierski, and W. Nazarewicz, *Nucl. Phys. A* **611**, 211 (1996).
- [28] M. Bender, K. Rutz, P.-G. Reinhard, J. A. Maruhn, and W. Greiner, *Phys. Rev. C* **60**, 034304 (1999).
- [29] M. Bender, W. Nazarewicz, and P.-G. Reinhard, *Phys. Lett. B* **515**, 42 (2001).
- [30] J. Berger, D. Hirata, and M. Girod, *Acta Phys. Pol. B* **34**, 1909 (2003).
- [31] A. V. Afanasjev and S. Frauendorf, *Phys. Rev. C* **71**, 24308 (2005).
- [32] S. E. Agbemava, A. V. Afanasjev, T. Nakatsukasa, and P. Ring, *Phys. Rev. C* **92**, 054310 (2015).
- [33] P. Möller, J. Nix, W. D. Myers, and W. J. Swiatecki, *Nucl. Phys. A* **536**, 61 (1992).
- [34] J. Dechargé, J.-F. Berger, K. Dietrich, and M. S. Weiss, *Phys. Lett. B* **451**, 275 (1999).
- [35] J.-F. Berger, L. Bitaud, J. Dechargé, M. Girod, and K. Dietrich, *Nucl. Phys. A* **685**, 1 (2001).
- [36] J. Dechargé, J. F. Berger, M. Girod, and K. Dietrich, *Nucl. Phys. A* **716**, 55 (2003).
- [37] J. C. Pei, F. R. Xu, and P. D. Stevenson, *Phys. Rev. C* **71**, 034302 (2005).
- [38] A. D. Becke and K. E. Edgecombe, *J. Chem. Phys.* **92**, 5397 (1990).
- [39] A. Savin, R. Nesper, S. Wengert, and T. F. Fässler, *Angew. Chem. Int. Ed. Engl.* **36**, 1808 (1997).
- [40] A. Scemama, P. Chaquin, and M. Caffarel, *J. Chem. Phys.* **121**, 1725 (2004).
- [41] M. Kohout, *Int. J. Quantum Chem.* **97**, 651 (2004).
- [42] T. Burnus, M. A. L. Marques, and E. K. U. Gross, *Phys. Rev. A* **71**, 10501 (2005).
- [43] J. Poater, D. M., M. Solà, and B. Silvi, *Chem. Rev.* **105**, 3911 (2005).
- [44] P.-G. Reinhard, J. A. Maruhn, A. S. Umar, and V. E. Oberacker, *Phys. Rev. C* **83**, 34312 (2011).
- [45] C. L. Zhang, B. Schuetrumpf, and W. Nazarewicz, *Phys. Rev. C* **94**, 064323 (2016).
- [46] B. Schuetrumpf, C. Zhang, and W. Nazarewicz, in *Nuclear Particle Correlations and Cluster Physics* (World Scientific, 2017) Chap. 5, p. 135.
- [47] DIRAC, a relativistic ab initio electronic structure program, Release DIRAC15 (2015), written by R. Bast *et al.* (see <http://www.diracprogram.org>).
- [48] K. G. Dyall, *J. Chem. Phys.* **100**, 2118 (1994).
- [49] M. Iliáš and T. Saue, *J. Chem. Phys.* **126** (2007).
- [50] K. G. Dyall, *Theor. Chem. Acc.* **115**, 441 (2006).
- [51] J. Sikkema, L. Visscher, T. Saue, and M. Iliáš, *J. Chem. Phys.* **131**, 124116 (2009).
- [52] K. G. Dyall, I. P. Grant, F. A. Parpia, and E. P. Plummer, *Comput. Phys. Commun.* **55**, 425 (1989).
- [53] V. P. Shevelko and A. V. Vinogradov, *Phys. Scr.* **19**, 275 (1979).
- [54] U. Hohm and K. Kerl, *Mol. Phys.* **69**, 803 (1990).
- [55] T. Nakajima and K. Hirao, *Chem. Lett. (Jpn.)*, 766 (2001).
- [56] T. Hangele and M. Dolg, *J. Chem. Phys.* **138**, 044104 (2013).
- [57] M. Bender, P.-H. Heenen, and P.-G. Reinhard, *Rev. Mod. Phys.* **75**, 121 (2003).
- [58] M. Kortelainen, J. McDonnell, W. Nazarewicz, P.-G. Reinhard, J. Sarich, N. Schunck, M. V. Stoitsov, and S. M. Wild, *Phys. Rev. C* **85**, 24304 (2012).
- [59] P. Klüpfel, P. G. Reinhard, T. J. Bürvenich, and J. A. Maruhn, *Phys. Rev. C* **79**, 034310 (2009).
- [60] P.-G. Reinhard, in *Computational Nuclear Physics I - Nuclear Structure*, edited by K. Langanke, S. Koonin, and J. Maruhn (Springer, Berlin, 1991) p. 28.